

Calibration of Photomultiplier Tubes for the Fluorescence Detector of Telescope Array Experiment using a Rayleigh Scattered Laser Beam

Shingo Kawana^{a,*}, Nobuyuki Sakurai^b, Toshihiro Fujii^b,
Masaki Fukushima^{c,d}, Naoya Inoue^a, John N. Matthews^e, Shoichi Ogio^b,
Hiroyuki Sagawa^c, Akimichi Taketa^{c,f}, Masato Takita^c, Stan B. Thomas^e,
Hisao Tokuno^{g,h}, Yoshiki Tsunesada^g, Shigeharu Udoⁱ,
Lawrence R. Wiencke^j

^a*Graduate School of Science and Engineering, Saitama University, Saitama 338-8570, Japan*

^b*Graduate School of Science, Osaka City University, Sumiyoshi, Osaka 558-8585, Japan*

^c*Institute for Cosmic Ray Research, University of Tokyo, Kashiwa, Chiba 277-8582, Japan*

^d*Institute for the Physics and Mathematics of the Universe, University of Tokyo, Kashiwa, Chiba 277-8582, Japan*

^e*Department of Physics and High Energy Astrophysics Institute, University of Utah, Salt Lake City, Utah 84112, USA*

^f*Earthquake Research Institute, University of Tokyo, Bunkyo-ku, Tokyo 113-0032, Japan*

^g*Graduate School of Science and Engineering, Tokyo Institute of Technology, Meguro, Tokyo 152-8551, Japan*

^h*Interactive Research Center of Science, Graduate School of Science and Engineering, Tokyo Institute of Technology, Meguro, Tokyo 152-8551, Japan*

ⁱ*Kanagawa University, Yokohama, Kanagawa 221-8624, Japan*

^j*Department of Physics, Colorado School of Mines, Golden, Colorado 80401, USA*

Abstract

We performed photometric calibration of the PhotoMultiplier Tube (PMT) and readout electronics used for the new fluorescence detectors of the Telescope Array (TA) experiment using Rayleigh scattered photons from a pulsed nitrogen laser beam. The experimental setup, measurement procedure, and

*Corresponding author. E-mail address: kawana@crsgm1.crinoue.phy.saitama-u.ac.jp (S. Kawana)

results of calibration are described. The total systematic uncertainty of the calibration is estimated to be 7.2%. An additional uncertainty of 3.7% is introduced by the transport of the calibrated PMTs from the laboratory to the TA experimental site.

Keywords: Ultra-high energy cosmic ray, Air fluorescence telescope, Calibration of photomultiplier, Rayleigh scattering

1. Introduction

The Telescope Array (TA) experiment is designed to observe extensive air showers caused by Ultra-High Energy Cosmic Rays (UHECRs), using air fluorescence telescopes and an air shower array installed in the west desert of Utah, USA [1, 2]. An important scientific objective of the TA experiment is to measure the energy spectrum of cosmic rays in the ultra-high energy region, where a cutoff structure generated by the interaction of UHECRs with the cosmic microwave background has been predicted by Greissen, Zatsepin and Kuzmin (GZK) [3, 4].

A measurement reported by the AGASA experiment in 1998 showed a spectrum that extended beyond the expected GZK cutoff [5, 6]. The HiRes experiment recently reported a strong suppression of cosmic ray flux [7] at around the predicted energy of $10^{19.7}$ eV [8], which was also observed by the Pierre Auger Observatory [9].

A precise measurement of the cutoff energy and the spectral shape around the cutoff is crucial to the identification of the origin of the observed structure, i.e., whether it is caused by the GZK effect or by some other mechanism such as the acceleration limit of cosmic rays. Answering this question is an

19 important objective of the TA experiment.

20 The TA consists of two different types of detectors. An air shower array
21 covers a ground area of about 700 km^2 with 507 scintillator Surface Detectors
22 (SDs) deployed in a grid of 1.2 km spacing. The spectral shape of UHECRs
23 can be measured with good accuracy by the SD. It is fully efficient for the
24 trigger and event reconstruction above $10^{18.8} \text{ eV}$. Three Fluorescence Detec-
25 tor (FD) stations, each with 12-14 fluorescence telescopes, view the sky over
26 the surface array from the periphery (Figure 1). The energies of UHECR
27 events can be reliably determined by the FD because it directly measures
28 the energy deposit in the atmosphere generated by air showers.

29 The energy determination by the FD is affected by several experimental
30 uncertainties such as the fluorescence spectrum and yield, the atmospheric
31 attenuation of fluorescence photons, the photometric calibration of the tele-
32 scope, and the missing energy carried away by high energy muons and neu-
33 trinos. In this paper, we address the third uncertainty, i.e., the photometric
34 calibration of the PMTs used for the FD camera.

35 One of the three FD stations of the TA, Middle Drum (MD), is located
36 to the north of the SD array (Figure 1). The telescopes at the MD site are
37 refurbished HiRes [10] telescopes. A calibration procedure similar to that
38 employed by HiRes using a xenon flasher was applied to the FDs in MD. The
39 role of MD is to import the established energy scale of previous experiments
40 (HiRes-1, HiRes-2, and Fly's Eye) to the TA.

41 The other two FD stations, i.e., Black Rock Mesa (BRM) in the southeast
42 and Long Ridge (LR) in the southwest, were newly produced for the TA
43 experiment [11]. A spherical mirror (diameter 3.3 m) and an imaging camera

44 (16 × 16 PMT matrix) are installed in the FDs of BRM and LR. The field of
45 view of one telescope is 18° in azimuth and 15.5° in elevation. A combination
46 of 6 × 2 telescopes at each station provides a field of view of 108° in azimuth
47 and 3°–33° in elevation.

48 For the new telescopes at BRM and LR, we calibrated a combination
49 of PMT and readout electronics using a pulsed UV light source developed
50 specially for this purpose. This system is composed of a pulsed nitrogen
51 laser and a gas-filled chamber in which laser photons are scattered by the
52 gas molecules and detected by a PMT to be calibrated. We call it CRAYS
53 (Calibration using RAYleigh Scattering). In this paper, we describe the
54 development of CRAYS and the absolute photometric calibration of the FD
55 camera PMTs via CRAYS.

56 **2. FD Camera and its Calibration**

57 A photograph of the PMT assembly used for the FD camera is shown in
58 Figure 2. The PMT (R9508, Hamamatsu Photonics) has a hexagonal photo-
59 sensitive window with the opposite side distance of 60 mm. The PMT has a
60 typical quantum efficiency of 27% for $\lambda = 337.1$ nm (the laser wavelength)
61 and a collection efficiency of 90% as reported by the manufacturer. The gains
62 of all the PMTs were adjusted at $\sim 6.0 \times 10^4$ as described later in this paper.
63 A UV transparent filter (BG3, Schott AG) of 4 mm thickness is attached to
64 the PMT window. Its transmittance is measured to be 89% for $\lambda = 337$ nm
65 [12].

66 The signal from the PMT is amplified by a factor of 52.7 at the PMT
67 base and is sent to a Signal Digitizer and Finder (SDF) module [13] using a

68 25 m long twisted pair cable. The waveform is digitized by a 12-bit, 40 MHz
69 Flash ADC (FADC) with 2.0 V full scale. Four consecutive digitizations of
70 the same input signal are summed together by the Field Programmable Gate
71 Array (FPGA) in the SDF, and the data of 14-bit dynamic range is read out.

72 The overall schematics of the FD PMT calibration at the TA is shown
73 in Figure 3. We calibrated 75 PMTs using CRAYS in a laboratory at the
74 Institute for Cosmic Ray Research (ICRR), University of Tokyo, in Japan.
75 The CRAYS-calibrated PMTs were transported to the TA experimental site
76 in Utah, and installed into the FD cameras - one calibrated PMT at the
77 center of each camera (Standard PMT) and another calibrated PMT toward
78 the corner of the camera to monitor the behavior of the Standard PMT. The
79 same High Voltage (HV), as determined by the CRAYS calibration at the
80 ICRR, was applied to the Standard PMT at the TA site. Using a diffused
81 xenon flasher [12] in situ, we adjusted the HVs of all other PMTs (255 units)
82 in the camera such that the gains of these PMTs are equal to the Standard
83 PMT.

84 All the PMTs calibrated via CRAYS have a small YAP light pulser (diam-
85 eter 4 mm) [14] embedded in a hole at the center of the BG3 filter (Figure 2).
86 The YAP is composed of a $\text{YAlO}_3\text{:Ce}$ scintillator with 50 Bq of ^{241}Am applied
87 on the surface. The YAP generates a light flash (wavelength ~ 350 nm; du-
88 ration ~ 30 ns) and produces approximately 450 photoelectrons in the PMT.
89 The gains of the PMTs calibrated via CRAYS in the laboratory have been
90 monitored in the field using the YAP signal.

91 3. CRAYS

92 The setup of CRAYS is shown in Figure 4. A pulsed laser beam is di-
93 rected into a scattering chamber filled with a high purity gas ($>99.999\%$)
94 consisting of a single molecular species, either N_2 or Ar. Scattered photons
95 from the beam illuminate a PMT viewing the chamber through a window.
96 Since the gas is very pure and the molecules in the gas are much smaller than
97 the wavelength used, the scattering process in the chamber is well described
98 by molecular (Rayleigh) scattering. The total number of photons in the laser
99 pulse is calculated from the energy measured by a calibrated energy probe
100 at the end of the beam line. The number of the Rayleigh scattered photons
101 is calculated using the cross-section formula, which has been experimentally
102 verified to an accuracy of $\sim 1\%$ [15] (Sections 8.1). With a typical setup of
103 CRAYS for nitrogen gas (laser intensity 200 nJ; gas pressure 1000 hPa), an
104 intensity of approximately 80 photons/cm² is obtained on the PMT window
105 (Section 6.1). Uncertainties of the CRAYS calibration are 0.3% (statistical),
106 7.2% (systematic), and 3.7% (from transport to TA site) as described in Sec-
107 tion 8. We note that the same CRAYS setup was also used with much lower
108 laser intensity for calibrating the IceCube PMTs in single photon counting
109 mode [16].

110 3.1. Light Source and Optics

111 We used a nitrogen laser (VSL-337ND-S, Laser Science, Inc.) as a light
112 source (wavelength 337.1 nm; duration 4 ns). The maximum energy is 300
113 μJ per pulse. The wavelength of the nitrogen laser matches that of the
114 brightest air fluorescence line in the atmosphere [17]. The diameter of the

115 laser beam was limited to ~ 1 mm by a set of irises at the exit of the laser and
116 at the entrance of the scattering chamber. A remote-controlled shutter in the
117 beam line prevented the laser light from entering the chamber, as required.
118 A Neutral Density (ND) filter was used to reduce the beam intensity. The
119 reflected beam by the ND filter was measured by a pyro-electric energy probe
120 (Rjp-435, Laser Probe, Inc.) that monitored the relative intensity of the
121 beam.

122 The nitrogen laser is inherently depolarized. To eliminate an elliptical
123 polarization introduced by the ND filter, a combination of a polarizer and a
124 retardation plate ($\lambda/4$) was used to convert the beam into a circular polar-
125 ization. The intensity of the beam in the scattering chamber was measured
126 using a silicon photodiode energy probe (Rjp-465, Laser Probe, Inc.) placed
127 at the end of the beam line. Both energy probes were calibrated with 5%
128 absolute accuracy by the manufacturer. The energy measured by Rjp-465
129 ranged from 190 nJ to 220 nJ with a typical pulse-to-pulse fluctuation of 3%
130 as shown in Figure 5.

131 *3.2. Scattering Chamber*

132 The cylindrical scattering chamber has a diameter of 500 mm. The inner
133 surface is anodized in black, and the inner wall is coated with non-reflective
134 black paper to suppress stray light. The chamber was evacuated to ~ 3 hPa
135 using a membrane vacuum pump (DAU-100, ULVAC, Inc.) before introduc-
136 ing the high purity scatterer gas. The differential pressure of the chamber
137 with respect to the atmospheric pressure was monitored by a capacitance
138 manometer (BOC EDWARDS, Barocel 600AB) and the temperature inside
139 the chamber was measured by a thermister thermometer.

140 The PMT to be calibrated was installed just outside the chamber, as
141 shown in Figure 4. The distance from the center of the chamber to the PMT
142 glass window was set to 312 mm. The PMT detects photons scattered by the
143 gas molecules near the center of the chamber at a scattering angle (θ) of 90° .
144 The aperture of the PMT is limited by a slit (width 38.9 mm; height 10 mm)
145 located 37.5 mm away from the beam line. The aperture is further limited
146 by a removable mask installed 7 mm in front of the PMT glass window.
147 Masks having a hole of 20.0 mm and 36.0 mm in diameter exposed only
148 the central part of the PMT window where the uniformity is expected to be
149 good. All chamber windows are made of CaF_2 with anti-reflection coating.
150 A transmittance greater than 99% for $\lambda = 337$ nm was measured by the
151 manufacturer.

152 *3.3. Electronics and DAQ*

153 We used the same data acquisition electronics and cables used at the TA
154 sites as much as possible with the exception of the high voltage power supply
155 of the PMT. We verified the applied HVs were the same at the CRAYS
156 calibration and at the TA sites, using a reference resistor and a digital multi-
157 meter. Data acquisition was controlled using a PC that generated a trigger
158 for the laser. The synchronization output of the laser was fed to the energy
159 probes, and the energy readings of each laser shot were recorded by the PC.
160 The pressure and the temperature of the chamber were also recorded for each
161 calibration run.

162 The waveform output from the PMT was transmitted to the digitizer
163 module (SDF) installed in a VME crate. The synchronization signal from
164 the laser was recorded by the SDF to define the signal integration interval

165 in the off-line analysis. For YAP data recording, a trigger was generated in
166 the SDF by the YAP signal itself. The DAQ rate was approximately 20 Hz
167 for the CRAYS run and 50 Hz for the YAP run.

168 4. Performance Check

169 Before using CRAYS for calibration, we made the following investigations
170 to ensure that the photons detected by the PMT originated from the Rayleigh
171 scattering of the laser beam and that the background photon was under
172 control. First, the polarization of the beam was measured by temporarily
173 inserting a rotatable polarization plate and recording the output of the energy
174 probes at different rotation angles. In Figure 6, the relative intensity of the
175 laser beam measured by the downstream energy probe is plotted with respect
176 to the change of the polarizer rotation angle ϕ . A fit to the sinusoidal curve

$$1 + A \sin 2(\phi + \phi_0) \quad (1)$$

177 was made with an amplitude A and a phase ϕ_0 as free parameters. The
178 obtained values, $A = -0.04$ and $\phi_0 = -8^\circ$, indicate an elliptical polarization
179 of 4% in the axis 37° away from the vertical-upward direction. An effect of
180 the polarization on the number of expected Rayleigh scattered photons in
181 the CRAYS setup is described in Section 8.2.

182 Next, the amount of the scattered photons and the PMT responses were
183 measured by changing the pressure of the gas between 3 and 1013 hPa.
184 The integration of the FADC signal and the pedestal subtraction were done
185 in the same manner as described in Sections 6.2 and 7. The result of the
186 measurements for nitrogen and argon gas are shown in Figure 7. Good

187 linearities of the PMT output with respect to the change of the gas pressure
 188 were obtained both for nitrogen and argon. The argon to nitrogen ratio
 189 (Ar/N_2) was 0.857 ± 0.007 from a linear fit to the measured FADC counts and
 190 taking a ratio of the two slopes. The measured ratio is in a good agreement
 191 with the theoretical cross-section calculation, which predicts a value of 0.849
 192 (Section 8.1).

193 A signal of 16-photons-equivalent was detected in the vacuum setup. This
 194 is about 1.9% of the Rayleigh scattered photons for the laser energy of 200 nJ,
 195 measured with the PMT mask of 36 mm ϕ (nitrogen gas; pressure, 1000 hPa).
 196 This background without scatterer molecules in the CRAYS chamber was
 197 attributed to the stray light generated by reflection of the laser by beam line
 198 elements such as the CaF_2 window and the energy probe. The background
 199 amount was stable during the calibration runs, and its contribution to the
 200 PMT signal was subtracted in the data analysis.

201 Finally, a linear polarization was artificially introduced in the beam line
 202 using the rotatable polarization plate, and the PMT signal was measured for
 203 different polarization angles. The measurement was made for nitrogen gas.
 204 Figure 8 shows a change of the integrated FADC count for different settings
 205 of the rotation angle (ϕ) of the polarization plate between 0° and 180° , where
 206 ϕ is defined to be zero in the vertical-upward direction. The data points are
 207 fitted with a sinusoidal function [18],

$$A \left[\frac{1 + \rho_0}{2 + \rho_0} - \frac{1 - \rho_0}{2 + \rho_0} \cos 2(\phi + \phi_0) \right] + B \quad (2)$$

208 where an amplitude A , a background B , and a phase ϕ_0 are free parameters,
 209 and a depolarization ratio, ρ_0 , is introduced as a constant of 0.022 (Section 8).
 210 We obtained $A = 980.1$, $B = 8.1$, $\phi_0 = -89.2^\circ$ with $\chi^2/\text{NDF} = 22.9/16$.

211 The minimum value at $\phi = -\phi_0$ is 3.0 % of the maximum value, which is
212 attributed to a depolarization effect of diatomic nitrogen gas (2.2 %) and the
213 unpolarized background (0.8%).

214 5. Calibration Procedure

215 We calibrated a total of 75 PMT assemblies with CRAYS. The procedure
216 is listed below.

- 217 1. A relation between the PMT gain and the applied HV was measured
218 by pulsing a UV LED, installed in the chamber opposite to the PMT
219 (Figure 4). A set of LED runs were carried out in a range between -700
220 V and -1250 V. The integrated FADC counts X and the HV setting
221 Y are well fitted with a function $X = \alpha Y^\beta$, yielding a measurement of
222 the parameter $\beta = 8.1 \pm 0.4(\text{rms})$.
- 223 2. Next, several laser runs were made for each PMT to determine the HV
224 setting for the calibration. The scattering chamber was filled with ni-
225 trogen gas (~ 1010 hPa) and a PMT mask ($36 \text{ mm}\phi$) was attached. The
226 HV to be applied to each PMT was tuned iteratively using the gain-HV
227 relation (step-1) such that all the calibrated PMTs had approximately
228 the same integrated FADC counts (~ 360 counts for a 200 nJ laser
229 pulse). The average of the resultant HV settings for the 75 PMTs was
230 $-870 \pm 50(\text{rms})$ V.
- 231 3. By applying the HV determined (step-2), three CRAYS laser runs were
232 carried out to measure the PMT response with three different PMT
233 mask conditions: $20 \text{ mm}\phi$, $36 \text{ mm}\phi$, and no mask.

234 4. After the laser calibration, the YAP data was recorded with the same
235 HV setting for future reference.

236 For each CRAYS run, we collected the data of 2000 laser shots: 1000
237 shots with shutter-open and 1000 shots with shutter-closed. We alternated
238 the shutter status every 100 laser shots. The shutter-closed data was used to
239 subtract the electrical noise synchronized with the laser shots. The energy
240 probe readings were recorded for each laser shot. The temperature and pres-
241 sure of the gas inside the chamber were continuously monitored. The YAP
242 data was also taken for 2000 events.

243 The temperature in the laboratory where the CRAYS setup was installed
244 was maintained at $25 \pm 1^\circ\text{C}$ during the measurement, and the absolute at-
245 mospheric pressure was measured by a mercury pressure gauge for each cal-
246 ibration run.

247 6. Data Analysis

248 6.1. Photon Acceptance

249 The cross-section of Rayleigh scattering in nitrogen gas at $\lambda = 337.1$ nm
250 is given by the expression (Section 8.1)

$$\frac{d\sigma_R}{d\Omega} = \frac{3}{16\pi}(1 + \cos^2 \theta) \times 3.50 \times 10^{-26} \text{ cm}^2 \quad (3)$$

251 The molecular density N of the scatterers can be determined from the equa-
252 tion of state for the ideal gas,

$$PV = NRT \quad (4)$$

253 where P is the pressure, V is the volume, T is the temperature [K], and R
254 is the gas constant having a value of 8.31 [J/K/mol]. For nitrogen gas at

255 1000 hPa and 25°C, $N = 2.43 \times 10^{19} \text{ cm}^{-3}$. The minor correction for Van
256 der Waals gas can be neglected for our purpose.

257 A pulse of 200 nJ nitrogen laser beam includes 3.39×10^{11} photons.
258 With a Rayleigh scattering cross-section of $3.50 \times 10^{-26} \text{ cm}^2$, the number of
259 Rayleigh scattered photons along the beam line inside the chamber is $1.43 \times$
260 10^7 .

261 We performed ray tracing of Rayleigh scattered photons in the chamber in
262 order to estimate the number of photons accepted by the PMT. The Rayleigh
263 scattered photons were produced along the beam line with a scattering angle
264 dependence of $1 + \cos^2\theta$ and with uniform azimuthal angle dependence.
265 The generated photons were allowed to enter the PMT directly or with one
266 scattering on a chamber element such as the inner wall or the baffles. The
267 shadow of the YAP embedded in the BG3 filter was also taken into account.

268 The ray tracing MC simulation showed that the average number of pho-
269 tons that reached the PMT window was 823 for nitrogen gas at 1000 hPa
270 with a PMT mask of $36 \text{ mm}\phi$, and the laser intensity of 200 nJ. An effective
271 length of 48.8 mm of the laser beam line near the chamber center was seen
272 from the PMT. The photons entered normal to the PMT window within 8° ,
273 making a nearly uniformly irradiated circular area (diameter 36.6 mm) on
274 the PMT window.

275 The effect of stray light originating from the Rayleigh scattering by the
276 beam line was estimated by changing reflection coefficient of the chamber
277 inner walls. We used a measured reflectivity of 0.023 for the chamber inner
278 wall. For this value and assuming mirror scattering, three photons on aver-
279 age were detected after a single scattering on the chamber wall in addition

280 to the 823 photons of direct incidence. The number was less than one when
281 a random (isotropic) scattering was assumed. Because the scattering is ex-
282 pected to be close to Lambertian on the black paper covering a major part of
283 the chamber wall, we concluded that the effect of stray light originating from
284 the Rayleigh scattering in the beam line is negligible. The effect of multiple
285 scattering on the chamber wall was also tested to be negligible.

286 *6.2. Waveform Integration*

287 A typical digitized PMT waveform is shown in Figure 9. A time interval
288 of $51.2 \mu\text{s}$ was recorded centered on the PMT signal. The PMT signal was
289 detected within 100 ns of the laser synchronization signal (Figure 9). We
290 determined the range of signal integration to be $1 \mu\text{s}$ before and $2 \mu\text{s}$ after
291 the peak of the synchronization signal. The pedestal level was evaluated as an
292 average of $19.2 \mu\text{s}$ duration at the beginning of the recorded waveform, and it
293 was subtracted before integration. The accidental overlap of the YAP signal
294 in the pedestal evaluation interval was low ($\sim 0.1\%$), but when it happened,
295 it was recognized by looking at the pedestal histogram, and removed.

296 A typical distribution of integrated PMT signals is shown in Figure 10,
297 after correcting the FADC signal for the shot-to-shot fluctuation in the laser
298 energy (normalized to the average energy).

299 The signal resolution defined by σ/peak of the distribution is 8.5%, which
300 is attributed to the statistical fluctuation of photoelectrons received by the
301 first dynode ($\sim 7.0\%$), the single photoelectron resolution ($\sim 3\%$), and the
302 electronics noise contribution ($\sim 4\%$).

303 7. Results

304 The photometric calibration constant C of the PMT-electronics system
305 is defined as $C = N_\gamma/\Sigma_{\text{ADC}}$ where N_γ means the total number of photons
306 striking the PMT sensitive area and Σ_{ADC} means the sum of the recorded
307 FADC counts. We used the measured laser energy, gas temperature, and
308 pressure for calculating the N_γ to be detected by the PMT. We subtracted
309 the contribution of the shutter-closed state from the shutter-open state as a
310 background when calculating Σ_{ADC} .

311 The following set of parameters were obtained for each calibrated PMT.

- 312 1. operation HV setting
- 313 2. calibration constant, C , with 36 mm ϕ PMT mask
- 314 3. Σ_{ADC} with 20 mm ϕ PMT mask and without PMT mask, normalized
315 to 200 nJ laser energy.
- 316 4. Σ_{ADC} of the YAP pulser

317 The distribution of C for all the 75 calibrated PMTs with 36 mm ϕ PMT
318 mask is shown in Figure 11. The statistical accuracy of the calibration is
319 better than 0.3%. These values are used in the air shower analysis of the TA
320 as calibration constants. The average of 2.25 [photons/FADC count] in Fig-
321 ure 11 corresponds to the PMT amplification of 6.0×10^4 using all the known
322 optical and electrical parameters of the PMT camera system (Section2).

323 The ratios of Σ_{ADC} obtained for different mask settings are shown in
324 Figure 12 for 75 PMTs together with the Gaussian fitting. The expected
325 values of these ratios are 0.294 (20 mm ϕ -mask/36 mm ϕ -mask) and 2.73
326 (no-mask/36 mm ϕ -mask) from the 2-dimensional sensitivity scanning of the

327 PMT window [12]. The fitted peaks of Figure 12 are 0.291 and 2.65 respec-
 328 tively, and the measurements agreed with the expectation within 3%. The
 329 widths (σ/peak) of the two distributions, 3.4% for no-mask/36 mm ϕ -mask
 330 and 1.7% for 20 mm ϕ -mask/36 mm ϕ -mask, indicate the level of uniformity
 331 of the photo-sensitive area among the calibrated PMTs. The accuracy of the
 332 no-mask/36 mm ϕ -mask ratio is relevant for transmitting the calibration of
 333 the Standard PMT to other PMTs in a given camera, which were used for
 334 the observation without any mask, by using a diffused xenon flasher in situ.

335 8. Systematic Uncertainties

336 8.1. Rayleigh Scattering Cross-Section

337 The total Rayleigh scattering cross-section σ_R for a single molecule is
 338 given by (e.g. [19])

$$\sigma_R(\nu) = \frac{24\pi^3\nu^4}{N^2} \left(\frac{n_\nu^2 - 1}{n_\nu^2 + 2} \right)^2 F_K(\nu) \quad (5)$$

339 where ν is the wavenumber [1/wavelength], N is the molecular density, n_ν is
 340 the refractive index, and $F_K(\nu)$ is the King correction factor accounting for
 341 the anisotropy of scatterings by non-spherical molecules. In order to use the
 342 equation (5), the values of n_ν and N should be chosen in a consistent way
 343 (i.e. values under a same condition in temperature and pressure) because of
 344 the relation $(n_\nu^2 - 1)/(n_\nu^2 + 2) \propto N$ [20]. We use n_ν values at NTP (normal
 345 temperature and pressure, $T = 273.15$ K and $P = 1013.25$ hPa), and we take
 346 $N = 2.69 \times 10^{19}$ cm $^{-3}$ [21].

347 Peck and Khanna [22] gave an empirical formula for the refractive index

348 of nitrogen at NTP in the wavelength range 468 – 2060 nm as

$$10^8(n_\nu - 1) = 6855.200 + \frac{3.243157 \times 10^{14}}{1.44 \times 10^{10} - \nu^2} \quad (6)$$

349 where ν is in [1/cm]. Abjean *et al.* [23] made a similar expression for a
350 shorter wavelength range 181 – 254 nm,

$$10^8(n_\nu - 1) = 6998.749 + \frac{3.233582 \times 10^{14}}{1.44 \times 10^{10} - \nu^2} \quad (7)$$

351 Bates [24] gave an interpolation to cover the intermediate range for 254 –
352 468 nm in the same form as (6) and (7) as

$$10^8(n_\nu - 1) = 5989.242 + \frac{3.3632663 \times 10^{14}}{1.44 \times 10^{10} - \nu^2} \quad (8)$$

353 This well reproduces the data in the literature [25] in 238 – 490 nm. These
354 formulae and data are shown in Figure 13.

355 Larsen [26, 27] measured the refractive index of argon at NTP in 230 –
356 567 nm and gave an expression

$$\begin{aligned} \frac{3}{2} \left(\frac{n_\nu^2 - 1}{n_\nu^2 + 2} \right) = & 1.2098 \times 10^6 \left(\frac{0.208972}{0.87882 \times 10^{10} - \nu^2} \right. \\ & \left. + \frac{0.208972}{0.9100 \times 10^{10} - \nu^2} + \frac{4.925837}{2.69636 \times 10^{10} - \nu^2} \right) \quad (9) \end{aligned}$$

357 where ν is in [1/cm]. This is also shown in Figure 13, together with the
358 measurements in different wavelength ranges given in [28] and [29].

359 The empirical formulae for n_ν of nitrogen and argon well fit the data in
360 the wide range, including the wavelength of our interest $\lambda = 337.1$ nm. For
361 our calculation, we use the equation (8) for nitrogen and (9) for argon, which
362 are evaluated as $n_\nu(\text{N}_2) - 1 = 3.0865 \times 10^{-4}$ and $n_\nu(\text{Ar}) - 1 = 2.9119 \times 10^{-4}$,
363 respectively.

364 The values of the King correction factor for nitrogen have been derived
 365 from the measurements by Bridge and Buckingham [30], Alms *et al.* [31]. A
 366 widely used dispersion relation for the King correction factor of nitrogen was
 367 given by Bates [24] using these data and the calculations by Oddershede and
 368 Svendsen [32],

$$F_K(\nu) = 1.034 + 3.17 \times 10^{-12} \nu^2 \quad (10)$$

369 where ν is in [1/cm]. Since argon is of monoatomic molecule, $F_K(\text{Ar}) = 1$
 370 is expected. The measurement by Rudder and Bach [33] showed that the
 371 degree of depolarization is $\sim 10^{-5}$, and the deviation of $F_K(\text{Ar})$ from unity
 372 is 3×10^{-5} [34, 35].

373 Using the n_ν and $F_K(\nu)$ values described above, we obtained the total
 374 Rayleigh scattering cross-sections of nitrogen and argon at $\lambda = 337.1$ nm
 375 under NTP, as

$$\sigma_R(\text{N}_2) = 3.50 \times 10^{-26} \text{ cm}^2, \quad \sigma_R(\text{Ar}) = 3.00 \times 10^{-26} \text{ cm}^2 \quad (11)$$

376 We used these cross-sections in our ray-tracing simulation of scattered laser
 377 photons in the CRAYS chamber (equation (3)). The accuracies of $\sigma_R(\text{N}_2)$
 378 and $\sigma_R(\text{Ar})$ which come from uncertainties in n_ν and F_K (for nitrogen) are
 379 1% and 0.3%, respectively (see also [15]).

380 The argon to nitrogen ratio is $\sigma_R(\text{Ar})/\sigma_R(\text{N}_2) = 0.858$. The ratio that
 381 CRAYS measures at $\theta = 90^\circ$ becomes 0.849, being slightly affected by the
 382 modification of the differential cross section for diatomic molecules (N_2) [18].

383 Experimental verifications of the Rayleigh cross-section formula (5) for
 384 gases in optical and ultraviolet wavelengths is rather scarce. An old mea-
 385 surement by Shardanand and Rao [36] gave cross-section values for nitrogen

386 and argon at 5 wavelengths from 363.8 nm to 632.8 nm, which are in agree-
 387 ment from expectations within 1 ~ 5% (Figure 14). Naus and Ubachs firstly
 388 carried out a modern laboratory laser measurement of Rayleigh scattering
 389 cross-sections of nitrogen and argon in 560–650 nm with the cavity-ringdown
 390 technique [15, 37]. They compared their measured values of cross-section and
 391 the expectations from the formula (5) with n_ν evaluated with (6) (9) and
 392 $F_K(\nu)$ by (10), and concluded that the measured and the calculated cross-
 393 sections agree within an experimental uncertainty of 1%. They also gave an
 394 empirical expression for the Rayleigh cross-section in a form

$$\sigma_R(\nu) = \bar{\sigma}\nu^{4+\epsilon} \quad (12)$$

395 By fitting their measured values to (12) they obtained $\bar{\sigma} = 22.94 \times 10^{-45}$
 396 and $\epsilon = 62.4 \times 10^{-3}$ for nitrogen, and $\bar{\sigma} = 19.89 \times 10^{-45}$ and $\epsilon = 61.5 \times$
 397 10^{-3} for argon [15]. This experiment was followed by the measurements in
 398 shorter wavelengths, as Sneep and Ubachs in 470–490 nm [38], and Ityaksov,
 399 Linnartz and Ubachs in 198 – 270 nm [39]. Although there are few cross-
 400 section data available in the very vicinity of our interest, $\lambda = 337.1$ nm, the
 401 measured values both in the shorter and the longer wavelength ranges are in
 402 excellent agreement with the expectation from (5) within ~ 1%, and there
 403 is no evidence of non-validity of (5) at 337.1 nm.

404 8.2. Uncertainty of CRAYS

405 A list of systematic uncertainties for the calibration constant, C ($36 \text{ mm}\phi$),
 406 obtained by CRAYS is given in Table 1. The calibration of PMTs with
 407 CRAYS is fully dependent on an evaluation of the total and differential cross-
 408 sections of Rayleigh scattering, σ_R and $d\sigma_R/d\Omega$, and its modification due to

409 the polarization of the incident laser beam. As described in Section 8.1,
 410 the direct measurement of σ_R agrees with the calculation within $\sim 1\%$ in the
 411 shorter and in the longer wavelength ranges around 337.1 nm. Using CRAYS,
 412 we measured the argon-to-nitrogen ratio at $\lambda = 337.1$ nm and showed that
 413 the calculation and the measurement of the ratio agree also within 1% (Sec-
 414 tion 4). This measurement gives an additional support that our calculation
 415 of σ_R is valid at the wavelength of 337.1 nm: no unexpected phenomena
 416 (as resonant absorptions) happened to the nitrogen laser photons in nitrogen
 417 gas.

418 The differential cross-section, $d\sigma_R/d\Omega$, for diatomic molecules such as
 419 N_2 is modified by a small amount from the equation (3), which we used
 420 for estimating the number of Rayleigh-scattered photons entering the PMT
 421 (Section 6.1). This modification factor at $\theta = 90^\circ$ is $2(1 + \rho_0)/(2 + \rho_0)$,
 422 or 1.011 using $\rho_0 = 0.022$ for the depolarization ratio of N_2 gas induced
 423 by the incident light of wavelength 337.1 nm. For monoatomic molecules
 424 such as argon, the depolarization ratio is zero and $d\sigma_R/d\Omega$ is calculated by
 425 equation (3). For nitrogen gas, we observed the depolarization effect in the
 426 CRAYS setup as described in Section 4. We assign a systematic uncertainty
 427 of +1.1% for $d\sigma_R/d\Omega$.

428 We observed an elliptical polarization of 4% for the incident laser beam
 429 with its polarization axis pointing 37° away from the vertical-upward direc-
 430 tion (Section 4, Figure 6). Rayleigh scattering of linearly polarized (100%)
 431 laser beam at $\theta = 90^\circ$ modifies the cross-section by a factor of $2(1 - \cos^2\alpha)$,
 432 where α is the rotation angle of the scattered photon measured from the
 433 direction of the polarization [18]. The α is 53° for the CRAYS setup whereas

434 $\alpha = 45^\circ$ corresponds to zero correction on the cross-section. The observed
435 polarization of 4% gives a correction factor of 1.000 ± 0.014 on the cross-
436 section, corresponding to $\alpha = 45 \pm 10^\circ$. We assign a systematic uncertainty
437 of 1.4% for the polarization effect.

438 In summary, for the systematic uncertainty of Rayleigh scattering cross-
439 section, we have ± 1.0 , $+1.1$, $\pm 1.4\%$ from σ_R , $d\sigma_R/d\Omega$ and the polarization.
440 We evaluate a total systematic uncertainty of 2.8%, taking a quadratic sum
441 for two \pm uncertainties and adding $+1.1\%$ uncertainty linearly.

442 The molecular density of the scatterer gas is calculated from the temper-
443 ature (T) and the pressure (P) of the gas inside the CRAYS chamber. We
444 evaluate an error of 1.3% for the molecular density calculation, consisting
445 of the absolute calibration of the mercury barometer (0.5%), the stability of
446 the pressure gauge calibration (1.0%), and the difference of the room tem-
447 perature and the gas temperature in the scattering chamber (maximum 2°C
448 corresponding to 0.7%).

449 The largest contribution to the systematic uncertainty comes from the
450 absolute calibration of the energy probe [40]. The manufacturer calibrated
451 the probes with an absolute accuracy of 5% using NIST traceable standards.
452 We used two Rjp-465 probes and the results were well within the quoted
453 accuracy. The second largest contribution comes from the acceptance cal-
454 culation, which is dominated by the measurement accuracy of the slit size
455 (38.9 ± 0.5 mm) and the distance from the laser beam line to the PMT mask
456 (312 ± 3 mm) including the inaccuracy of the laser beam position in the scat-
457 tering chamber. We estimated a total uncertainty of the acceptance to be
458 3.0%.

Table 1: Systematic uncertainties of the CRAYS calibration.

	Error
Cross-section (σ_R , $d\sigma_R/d\Omega$ and polarization)	2.8%
Molecular density (T and P)	1.3%
Measurement of laser energy	5.0%
Geometric aperture calculation	3.0%
Signal integration (Σ_{ADC})	2.0%
Background and noise subtraction (Σ_{ADC})	1.9%
Effect of geomagnetism	1.0%
Total (quadratic sum of above)	7.2%

459 The uncertainty of Σ_{ADC} is estimated as 2.0 % from the signal integration
 460 and 1.9 % from the background noise contribution. The uncertainty of signal
 461 integration (2%) is determined from the change of Σ_{ADC} by using a different
 462 method of estimating the pedestal level, and by using different signal integra-
 463 tion intervals. The uncertainty of background and noise subtraction (1.9%)
 464 is taken from the remaining Σ_{ADC} for the zero chamber pressure run. It is
 465 a conservative estimate because the amount of the background was stable
 466 throughout the calibration, and its contribution was actually subtracted in
 467 the data analysis. An uncertainty of 1.0% was estimated for the geomagnetic
 468 effect from the change of Σ_{ADC} for the YAP run taken in different azimuthal
 469 orientations.

470 All added in quadrature, we determined that the total systematic uncer-
 471 tainty of the CRAYS calibration is 7.2%.

472 *8.3. Transport of the Calibrated PMT*

473 Fifty PMTs with a YAP scintillator were calibrated in January 2008 in a
474 laboratory of the Institute for Cosmic Ray Research (ICRR), University of
475 Tokyo¹. They were then transported to the TA site in Utah and installed in
476 the 24 FD cameras in March 2008. Twenty two cameras had two calibrated
477 PMTs installed and two cameras had three calibrated PMTs. The same
478 nominal HV setting used in CRAYS calibration was applied to the Standard
479 PMT installed at the center of the camera, and the YAP signal was measured
480 again at the TA site. The signal obtained at the site was compared with that
481 measured during the calibration after correcting the temperature difference,
482 25°C during the calibration and $\sim 10^\circ\text{C}$ at the TA site, using the temperature
483 behavior of the YAP signal previously measured in the laboratory [41]. The
484 result is plotted in Figure 15 as the ratio of the two YAP measurements.
485 Only one PMT showed a large deviation of 0.85, which is attributable to a
486 change of the YAP light output ². The distribution in Figure 15, excluding
487 the outlier point (0.85), is fitted by a Gaussian with a mean of 0.999 and a
488 standard deviation of 0.037. The mean value of 0.999 indicates the stability of
489 the PMT gain from the laboratory calibration to the on-site installation. The
490 spread of 3.7% includes all the following uncertainties and differences in the
491 measurement: applied HVs, electronics sensitivities, temperature corrections,
492 geomagnetic effects in Japan and Utah, and possible drifts of YAP light
493 output and PMT gain during the transport.

¹A second batch of 25 PMTs were calibrated in August 2008

² Another calibrated PMT installed in the same camera had the ratio of 1.007, and the gain difference of these 2 PMTs was 2.3% as measured by a xenon flasher run.

494 **9. Summary**

495 Photometric calibration of the new fluorescence telescope of the TA was
496 carried out using CRAYS. Rayleigh scattering of nitrogen laser beam was
497 used for CRAYS to produce a short and uniform UV light flash of known
498 intensity on the PMT's photo-sensitive window. The Standard PMT for each
499 FD camera was calibrated with an absolute accuracy of 7.2% via CRAYS in
500 the laboratory. An additional uncertainty was introduced by the transport
501 of the calibrated PMTs from CRAYS to the experimental site in Utah. It is
502 estimated to be 3.7% using the YAP pulser.

503 **Acknowledgements**

504 We wish to thank the members of the Telescope Array (TA) collaboration
505 for making it possible (and necessary) to do this study. The TA experiment
506 is supported by the Japan Society for the Promotion of Science via Grants-
507 in-Aid for Scientific Research on Specially Promoted Research (21000002)
508 "Extreme Phenomena in the Universe Explored by Highest Energy Cosmic
509 Rays," and the Inter-University Research Program of the Institute for Cos-
510 mic Ray Research; by the U.S. National Science Foundation awards PHY-
511 0307098, PHY-0601915, PHY-0703893, PHY-0758342, PHY-0848320 (Utah),
512 and PHY-0649681 (Rutgers); by the National Research Foundation of Korea
513 (2006-0050031, 2007-0056005, 2007-0093860, 2010-0011378, 2010-0028071,
514 R32-10130); by the Russian Academy of Sciences (RFBR grants 10-02-01406a
515 and 11-02-01528a (INR)), IISN project No. 4.4509.10; and the Belgian Sci-
516 ence Policy under IUAP VI/11 (ULB). We also wish to thank the people and
517 officials of Millard County, Utah, for their wholehearted support. We grate-

518 fully acknowledge the contributions from the technical staffs of our home
519 institutions and the Center for High Performance Computing (CHPC), Uni-
520 versity of Utah.

521 **References**

- 522 [1] The Telescope Array Project: Design Report, July, 2000.
- 523 [2] H. Sagawa for the Telescope Array Collaboration, Proceedings of the
524 31st International Cosmic Ray Conference, Łódź, Poland (2009).
- 525 [3] K. Greisen, Phys. Rev. Lett. 16(1966) 748.
- 526 [4] T. Zatsepin and V.A. Kuzmin, JETP Lett. 4(1966) 78.
- 527 [5] M. Takeda, *et al.*, Phys. Rev. Lett. 81(1998) 1163.
- 528 [6] M. Takeda, *et al.*, Astropart. Phys. 19(2003) 447.
- 529 [7] R.U. Abbasi, *et al.*, Phys. Rev. Lett. 100(2008) 101101.
- 530 [8] V. Berezhinsky, A. Gazizov and S. Grigorieva, Phys. Rev. D74(2006)
531 043005.
- 532 [9] J. Abraham, *et al.*, Phys. Rev. Lett. 101(2008) 061101.
- 533 [10] T. Abu-Zayyad *et al.*, Nucl. Instrum. and Meth. A450(2000) 253.
- 534 [11] H. Tokuno *et al.*, arXiv:1201.0002v1, submitted to Nucl. Instrum. and
535 Meth. A.
- 536 [12] H. Tokuno *et al.*, Nucl. Instrum. and Meth. A601(2009) 364.

- 537 [13] A. Taketa *et al.*, in preparation.
- 538 [14] M. Kobayashi *et al.*, Nucl. Instrum. and Meth. A337(1994) 355.
- 539 [15] H. Naus and W. Ubachs, Opt. Lett., 25(2000) 347.
- 540 [16] R. Abbasi *et al.*, Nucl. Instrum. and Meth. A618(2010) 139.
- 541 [17] F. Arqueros, J. Hoerandel and B. Keilhauer, Nucl. Instrum. and Meth.
542 A597(2008) 1 and references therein.
- 543 [18] R.B. Miles, W.R. Lempert and J.N. Forkey, Meas. Sci. Technol.
544 12(2001) R33.
- 545 [19] A. Bucholtz, Appl. Opt., 34(1995) 2765.
- 546 [20] J.D. Jackson, Classical Electrodynamics 3rd ed., John-Wiley & Sons
547 (1999)
- 548 [21] P.J. Mohr, B.N. Taylor and D.B. Newell, Rev. Mod. Phys., 80(2008)
549 633.
- 550 [22] E.R. Peck and B.N. Khanna, J. Opt. Soc. Am., 56(1966) 1059.
- 551 [23] R. Abjean *et al.*, C. R. Acad. Sci. B, 271(1970) 411.
- 552 [24] D.R. Bates, Planetary and Space Science, 32(1984) 785.
- 553 [25] M.J. Weber, Handbook of Optical Materials, CRC press (2003).
- 554 [26] T. Larsen, Z. Physik, 98(1936) 17.
- 555 [27] P.J. Leonard, Atomic Data and Nuclear Data Tables, 14(1974) 21.

- 556 [28] E.R. Peck and D.J. Fisher, *J. Opt. Soc. Am.*, 56(1964) 1362.
- 557 [29] A. Bideau-Mehu *et al.*, *J. Quantitative Spectrosc. and Radiat. Transfer*,
558 25(1981) 395.
- 559 [30] N.J. Bridge and A.D. Buckingham, *Proc. R. Soc. A*, 295(1960) 424.
- 560 [31] G.R. Alms *et al.*, *J. Chem. Phys.*, 63(1975) 3321.
- 561 [32] J. Oddershee and E.N. Svendsen, *Chem. Phys.*, 64(1982) 359.
- 562 [33] R.R. Rudder and D.R. Bach, *J. Opt. Soc. Am.*, 58(1968) 1260.
- 563 [34] C. Fröhlich and G.E. Shaw, *Appl. Opt.*, 19(1980) 1773.
- 564 [35] S.S. Srivastava *et al.*, *Adv. Space Res.*, 44(2009) 1058.
- 565 [36] Shardanand and A.D. Rao, NASA technical report, NASA-TN-D-8442
566 (1977).
- 567 [37] H. Naus and W. Ubachs, *Proc. Lasers and Electro-Optics Europe 2000*,
568 IEEE/IET Electronic Library (2003).
- 569 [38] M. Sneeep and W. Ubachs, *J. Quantitative Spectrosc. and Radiat.*
570 *Transfer*, 92(2005) 293.
- 571 [39] D. Ityaksov, H. Linnartz, and W. Ubachs, *Molecular Physics*,
572 106(2008) 2471.
- 573 [40] L. Wiencke, F. Arqueros, J. Compton, M. Monasor, D. Pilger and
574 J. Rosado, *Proceedings of the 31st International Cosmic Ray Confer-*
575 *ence, Łódź, Poland (2009)*, arXiv:1105.4016 [astro-ph].

- 576 [41] S. Ogio *et al.*, Proceedings of the 31st International Cosmic Ray Con-
577 ference, Łódź, Poland (2009).

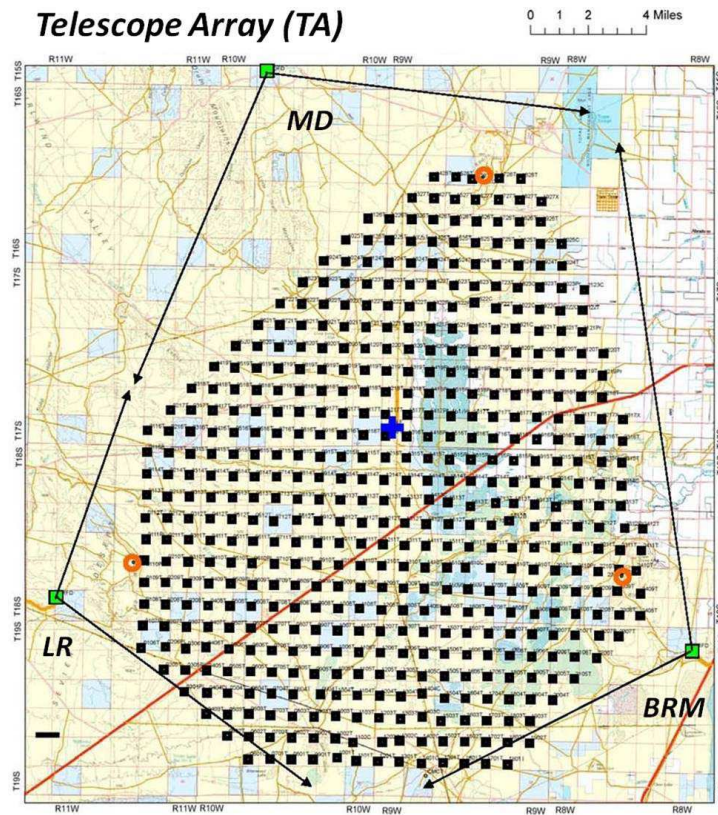


Figure 1: Detector layout of the TA experiment. The filled squares indicate the locations of the SDs. Three hollow squares, forming a triangle surrounding the SD array, show the locations of the FD telescope stations; the extent of their azimuthal field of view is indicated by arrows.

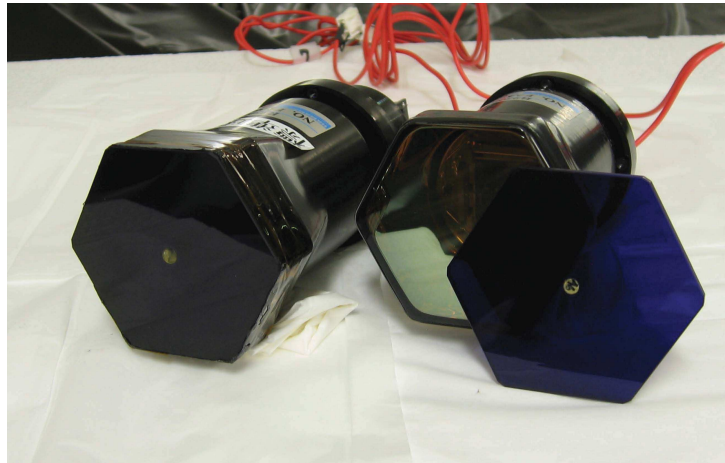


Figure 2: PMT assembly of the TA's new FD cameras calibrated by CRAYS. The BG3 filter contacts the PMT glass window with a thin air gap. On the right, the BG3 filter is removed from the PMT. An embedded YAP pulser can be seen at the center of the BG3 filter.

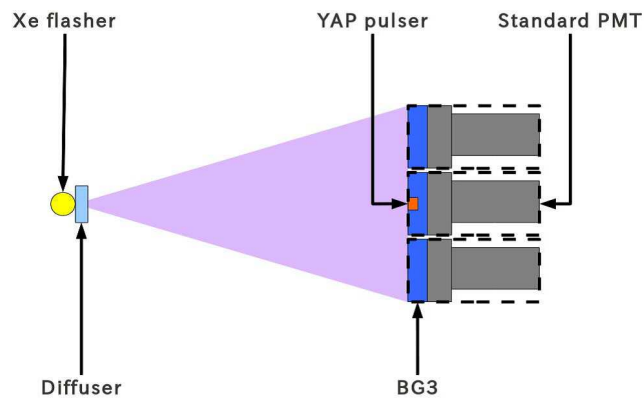


Figure 3: Schematics of the FD camera calibration at the TA experimental site. All the 256 PMTs in each camera were illuminated by the diffused xenon flasher. Only 3 PMTs were drawn in the schematics for simplicity.

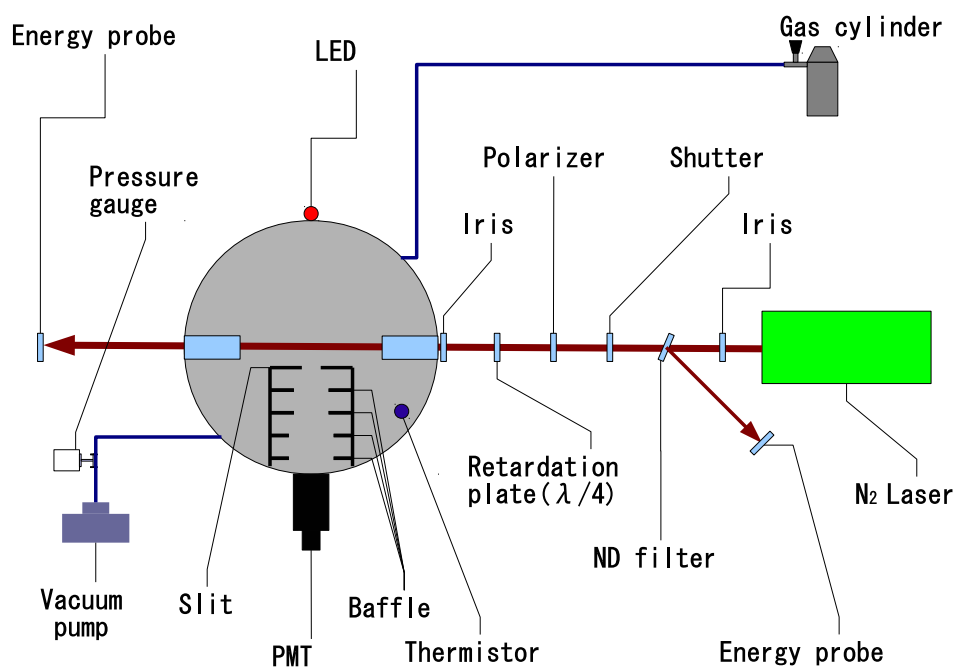


Figure 4: Measurement setup of CRAYS.

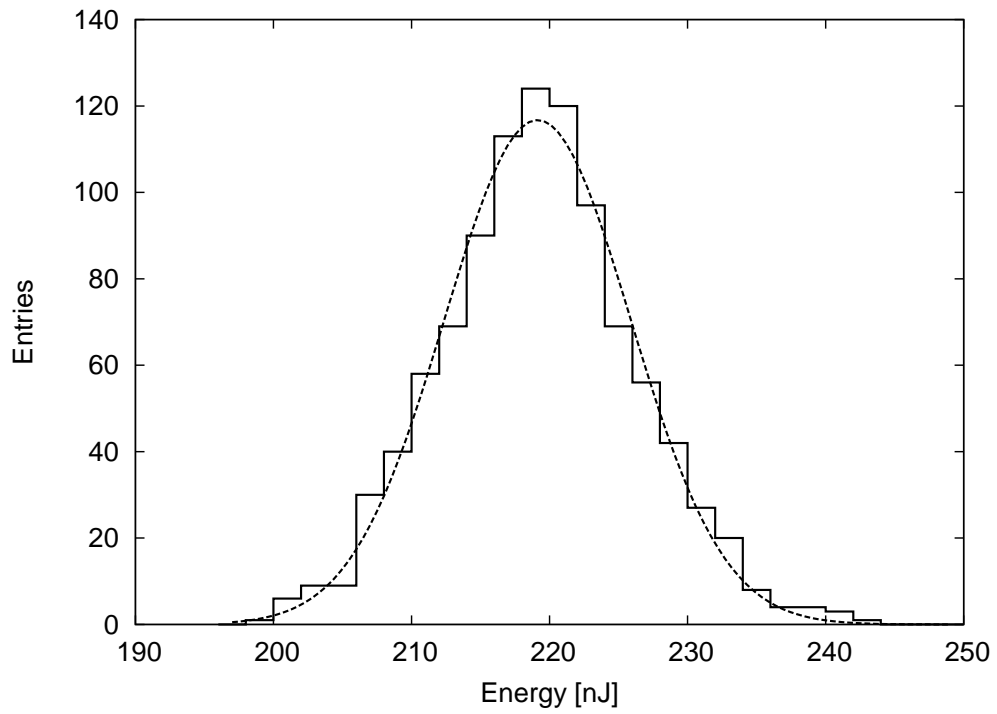


Figure 5: Distribution of the laser energies for one calibration run. A fit to the Gaussian is shown in the dashed line ($\sigma/\text{peak}=0.031$).

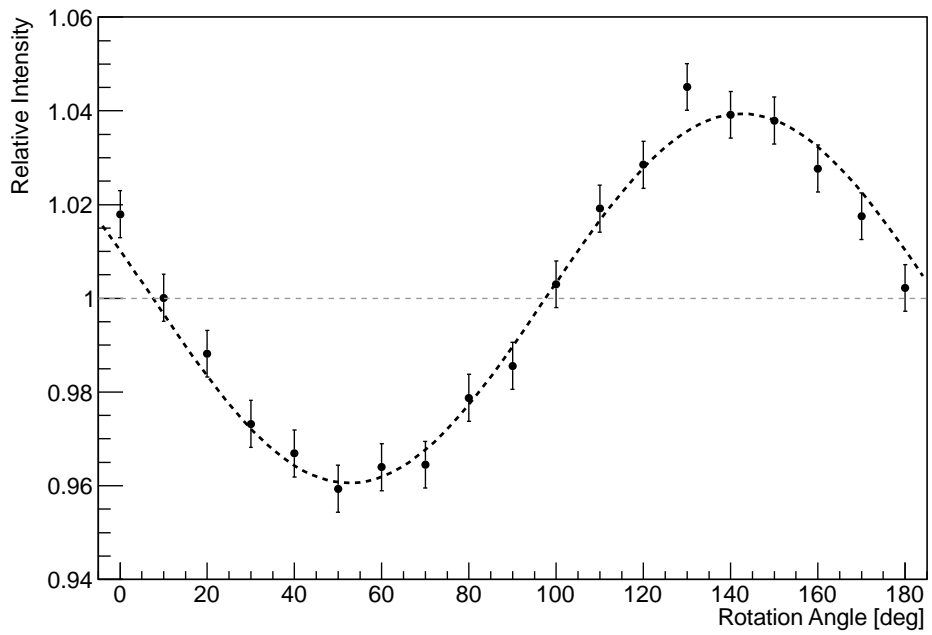


Figure 6: Relative change of the measured laser energy with respect to the polarizer rotation angle. A fit to the sinusoidal function is shown in the dashed line.

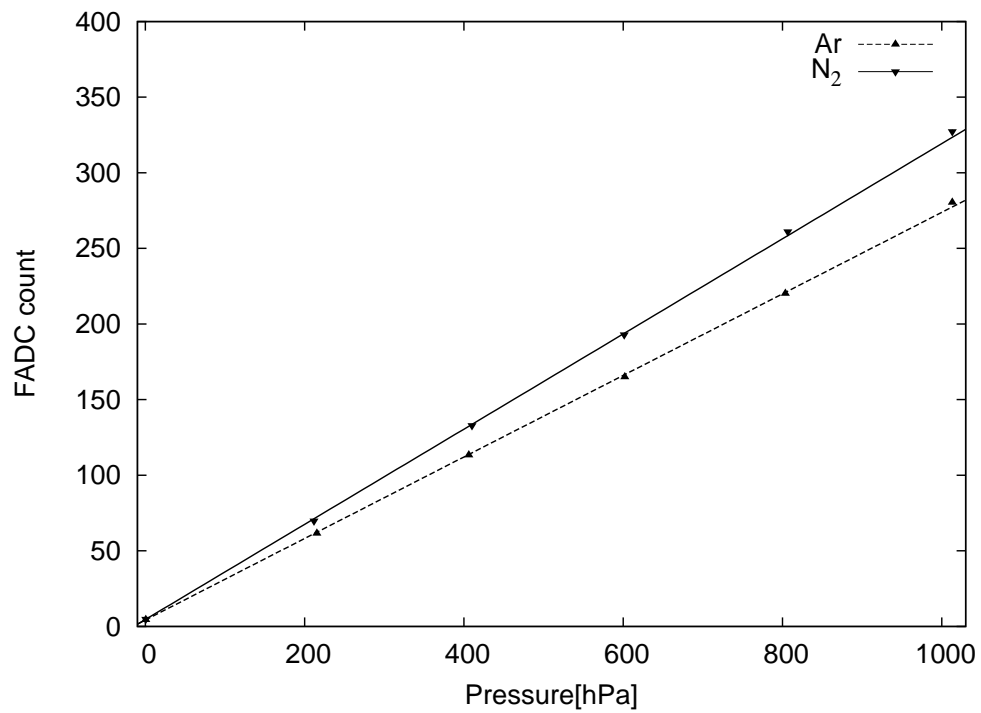


Figure 7: Integrated FADC counts generated by the photons scattered from the laser beam with respect to the change in gas pressure. A linear fit is shown in the solid line (nitrogen) and in the dashed line (argon).

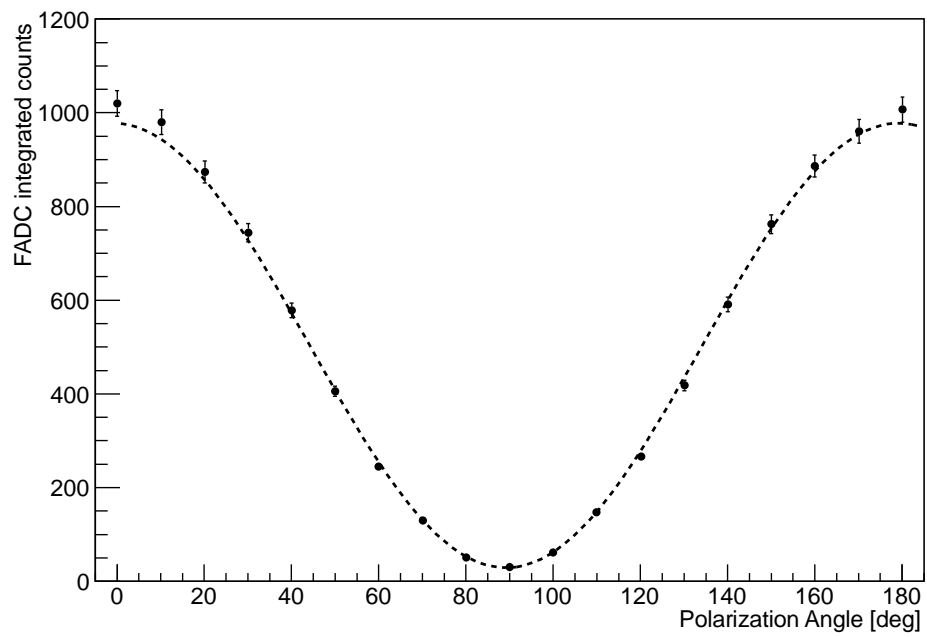


Figure 8: Integrated FADC counts generated by the photons scattered from the polarized laser beam with respect to the change of polarization angle. A fit to the sinusoidal function is shown in the dashed line.

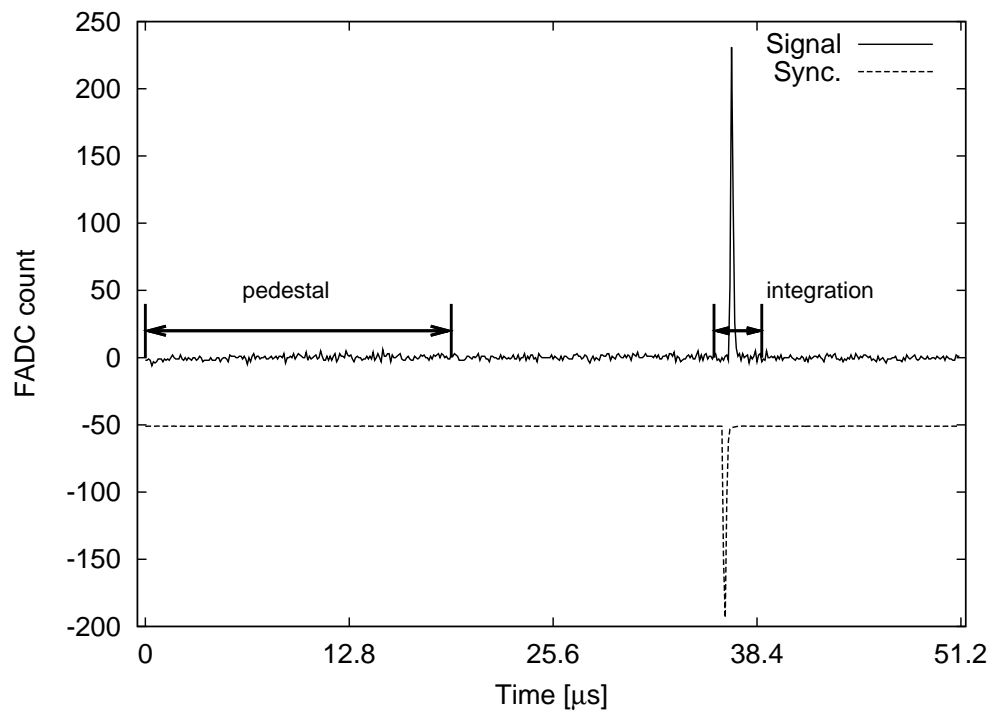


Figure 9: Typical PMT waveform from CRAYS. The time intervals for the pedestal determination and the signal integration are indicated. The laser synchronization signal (dashed line) is inverted.

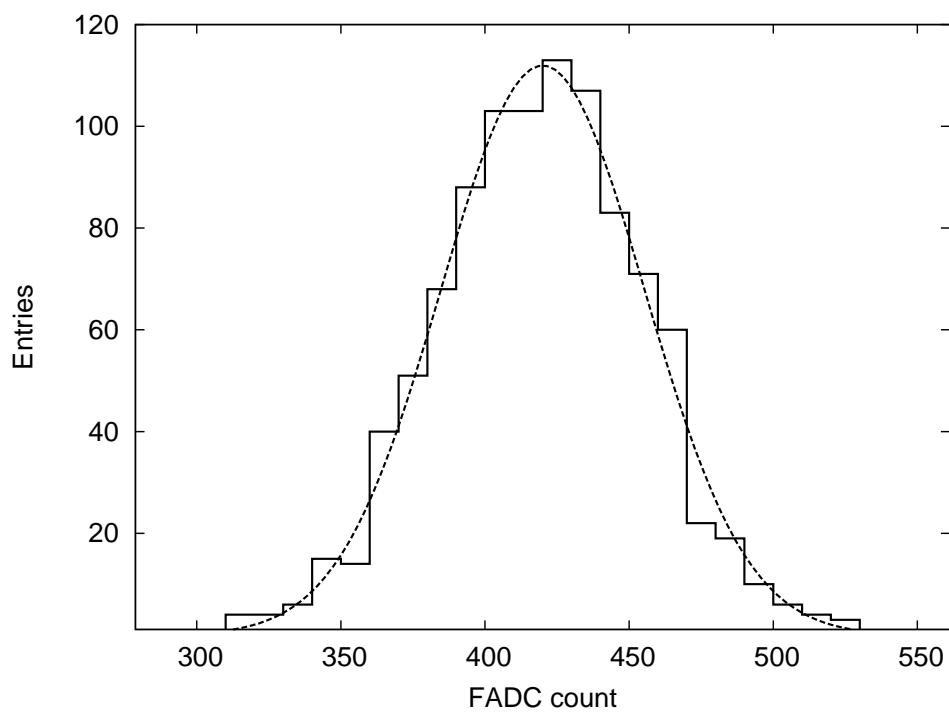


Figure 10: Distribution of the Σ_{ADC} for a CRAYS calibration run. A fit to the Gaussian is shown in the dashed line ($\sigma/\text{peak}=0.085$).

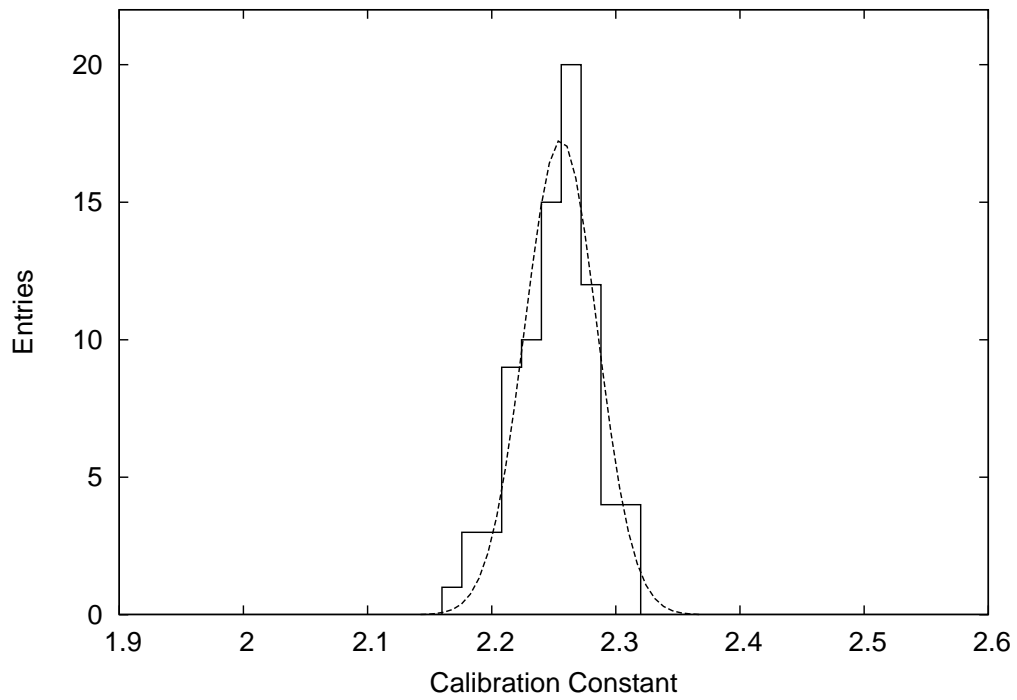


Figure 11: Distribution of the calibration constant, C , for 75 calibrated PMTs (36 mm ϕ mask). A fit to the Gaussian is shown in the dashed line (peak=2.256, σ =0.0291).

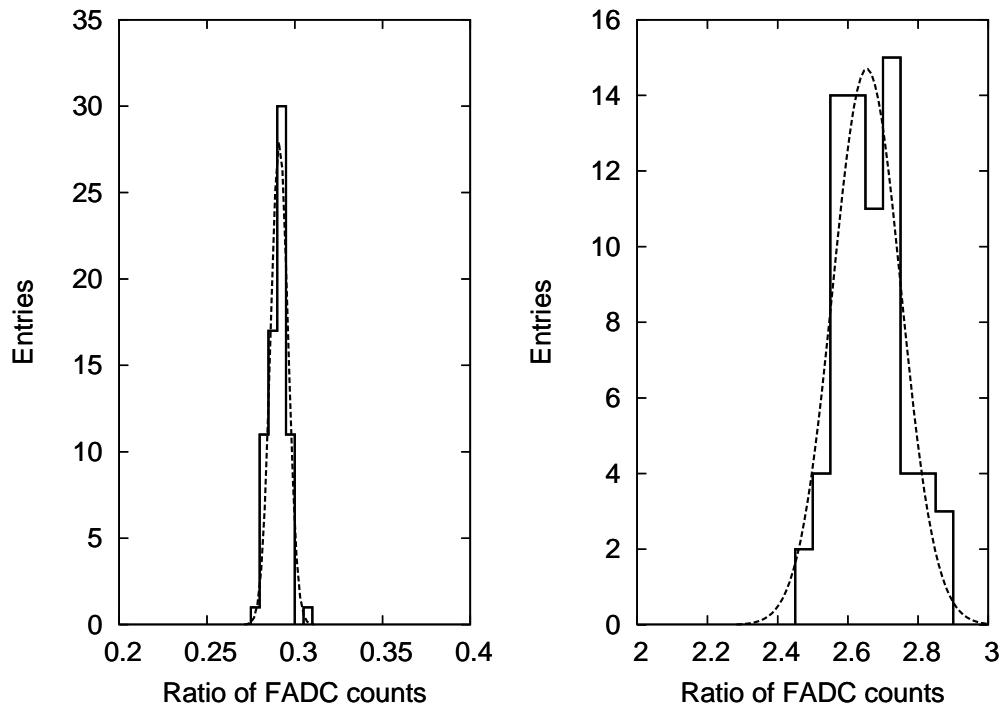


Figure 12: Distribution of the ratio of Σ_{ADC} for 75 PMTs; 20 mm ϕ -mask/36 mm ϕ -mask (left) and no-mask/36 mm ϕ -mask (right). A fit to the Gaussian is shown in the dashed line (peak = 0.291, $\sigma=0.050$ for the left, and peak = 2.65, $\sigma=0.097$ for the right).

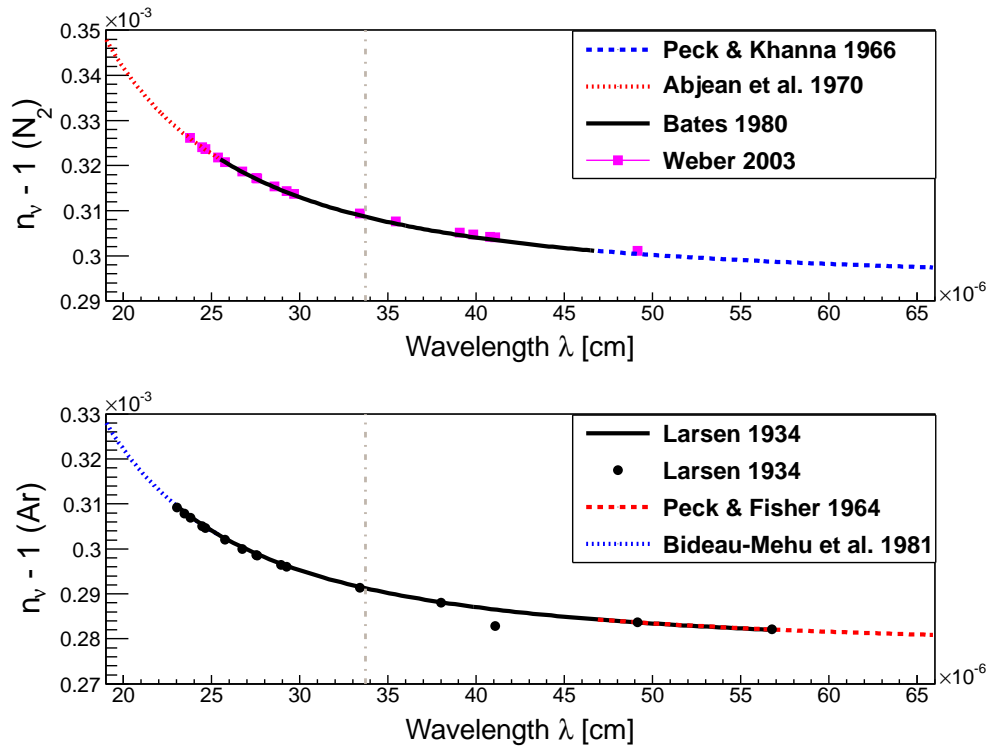


Figure 13: Refractive indices of nitrogen (upper) and argon (lower).

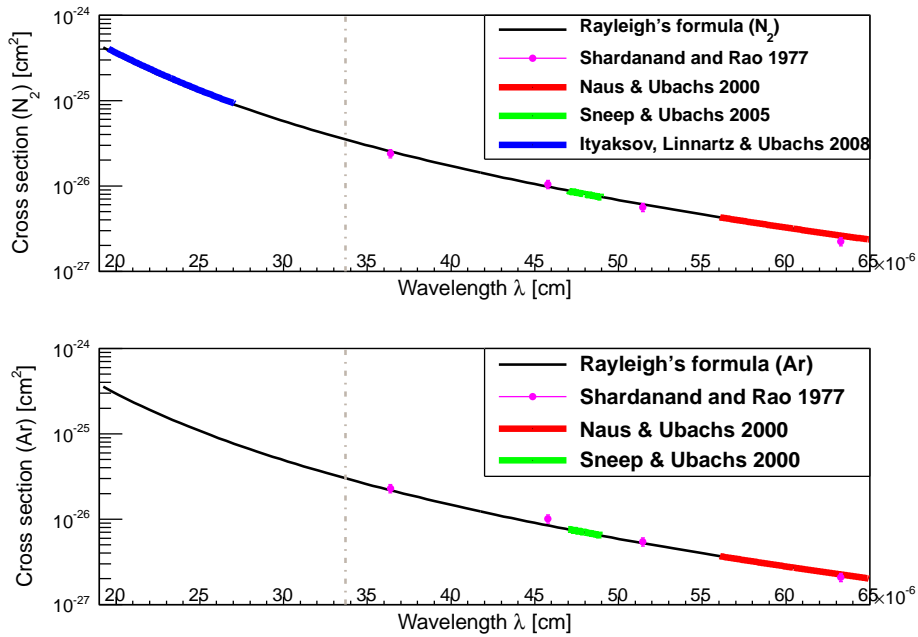


Figure 14: Rayleigh scattering cross-sections. The solid line is calculation by the formula (5) using the refractive indices and the King correction factor given in [24]. Fits for the experimental data given in the literature [15, 36–39] are shown in different colors.

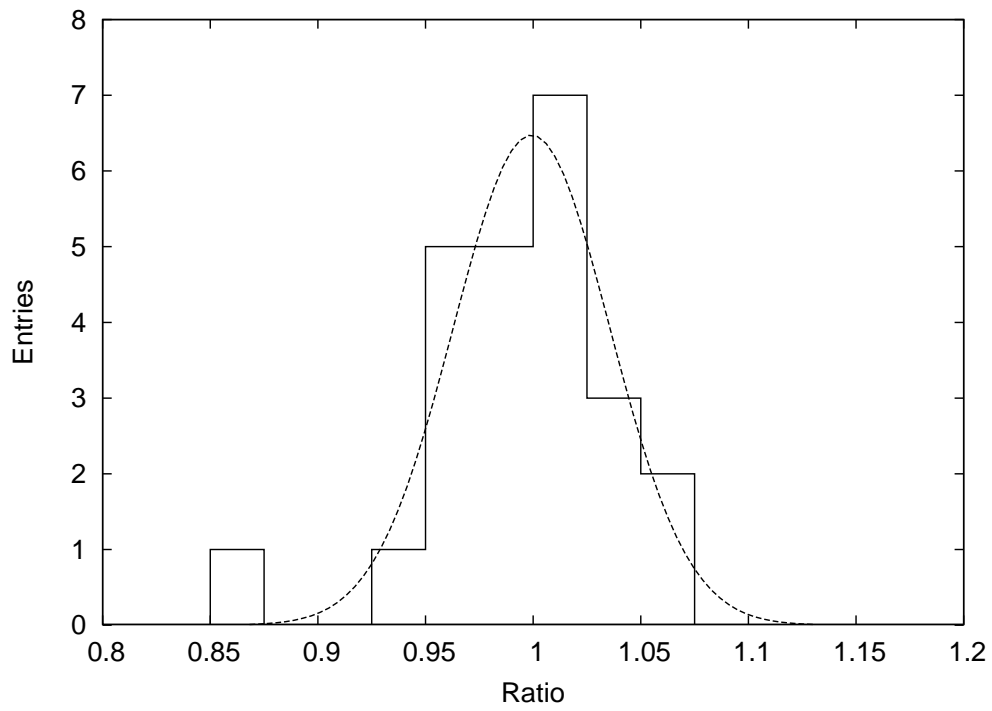


Figure 15: Change of the YAP signal from the laboratory calibration to the on-site use. A ratio (= on-site/lab.-calib.) is plotted for 24 Standard PMTs installed in the FD camera. A fit to the Gaussian is shown in the dashed line (peak = 0.999, $\sigma=0.037$).